THE JOURNAL OF PHYSICAL CHEMISTRY A

Article

pubs.acs.org/JPCA

Structure and Dissociation Pathways of Protonated Tetralin (1,2,3,4-Tetrahydronaphthalene)

Martin Vala*

Department of Chemistry and Center for Chemical Physics, University of Florida, Gainesville, Florida 32611-7200, United States

Jos Oomens and Giel Berden

Radboud University, Institute for Molecules and Materials, FELIX Laboratory, Toernooiveld 7c, NL-6525 ED Nijmegen, The Netherlands

ABSTRACT: The infrared multiple-photon dissociation (IRMPD) spectrum of protonated tetralin (1,2,3,4-tetrahydronaphthalene, THN) has been recorded using an infrared free electron laser coupled to a Fourier transform ion cyclotron mass spectrometer. IR-induced fragmentation of the protonated parent $[THN + H]^+$, m/z 133, yielded a single fragment ion at m/z 91. No evidence for fragment ions at m/z 131 or 132 was observed, indicating that protonated THN ejects neither atomic H nor molecular H_2. Comparison of the experimental spectrum with density functional calculations (B3LYP/6-311++G(d,p)) of the two possible protonated isomers identifies a preference for the position of protonation. Possible decomposition pathways starting from both $[THN + H(5)]^+$ and $[THN + H(6)]^+$ are investigated. The potential energy profiles computed for these decomposition routes reveal that (1) the m/z 91 ionic product resembles the benzylium ion, but with the extra hydrogen and the methylene substituents in various *ortho*, *meta*, and *para* conformations around the aromatic ring and that (2) the decomposition process involving the $[THN + H(6)]^+$ isomer is predominant, while the one involving the $[THN + H(5)]^+$ may play a smaller role. Potential energy pathways from the initial decomposition product(s) to the benzylium and tropylium ions have also been computed. Given the relatively low barriers to these ions, it is concluded that the benzylium ion and, with sufficient activation, the tropylium ion plus neutral propene are the final products.

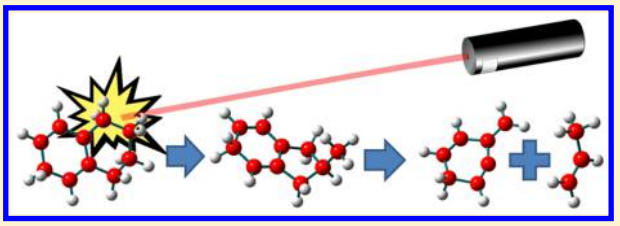

1. INTRODUCTION

Polycyclic aromatic hydrocarbons (PAHs) have been implicated in many of the chemical and physical phenomena occurring in the interstellar medium (ISM). From carriers of the unidentified infrared emission bands to the species responsible for the diffuse interstellar visible absorption bands, from building blocks of the fullerenes to catalysts for the production of molecular hydrogen, the PAHs have been much studied and their multifaceted roles in the ISM increasingly better understood. However, despite this progress, there are many aspects of their involvement that remain unexplored and unknown. One of these, the photostability of hydrogenated PAHs, has recently been noted by Schlathölter and co-workers to be largely unknown.[1] Indeed, experimental results suggest that the addition of hydrogen to PAHs changes their photostability.[2] This is an important topic since a number of recent studies by Mennella, Thrower, and Hornekær and co-workers have observed high superhydrogenation states in PAHs and demonstrated that hydrogen abstraction from these species can lead to molecular hydrogen production in the ISM.[3−5] A number of other mechanisms for the production of interstellar H_2 involving PAHs have also been proposed, computed, and experimentally investigated.[6−16]

Here, we confine ourselves to the question of whether further hydrogenation of a partially hydrogenated PAH will lead to greater H_2 production or to breakdown products. To address this question, we use a simple test system, the partially hydrogenated naphthalene molecule, 1,2-dihydronaphthalene (DHN), and its more completely hydrogenated cousin, tetralin (1,2,3,4-tetrahydronaphthalene, THN). In a previous investigation[16] protonated DHN (m/z 131) was found to dissociate along two channels yielding m/z 129 and m/z 91 products in approximately a 2:1 ratio. The primary channel yielded molecular hydrogen and an m/z 129 product, while the secondary channel resulted in an ionic m/z 91 product and a neutral C_3H_4 molecule. In this article, we extend this previous investigation to the decomposition of protonated tetralin.

2. EXPERIMENTAL AND COMPUTATIONAL METHODS

Infrared multiple photon dissociation (IRMPD) experiments on gaseous protonated tetralin were performed on a 4.7 T Fourier-transform ion cyclotron resonance mass spectrometer (FTICR-MS) coupled to a free electron laser with tunable

Received: February 25, 2017
Revised: May 25, 2017
Published: June 2, 2017

DOI: 10.1021/acs.jpca.7b01858
J. Phys. Chem. A 2017, 121, 4606−4612

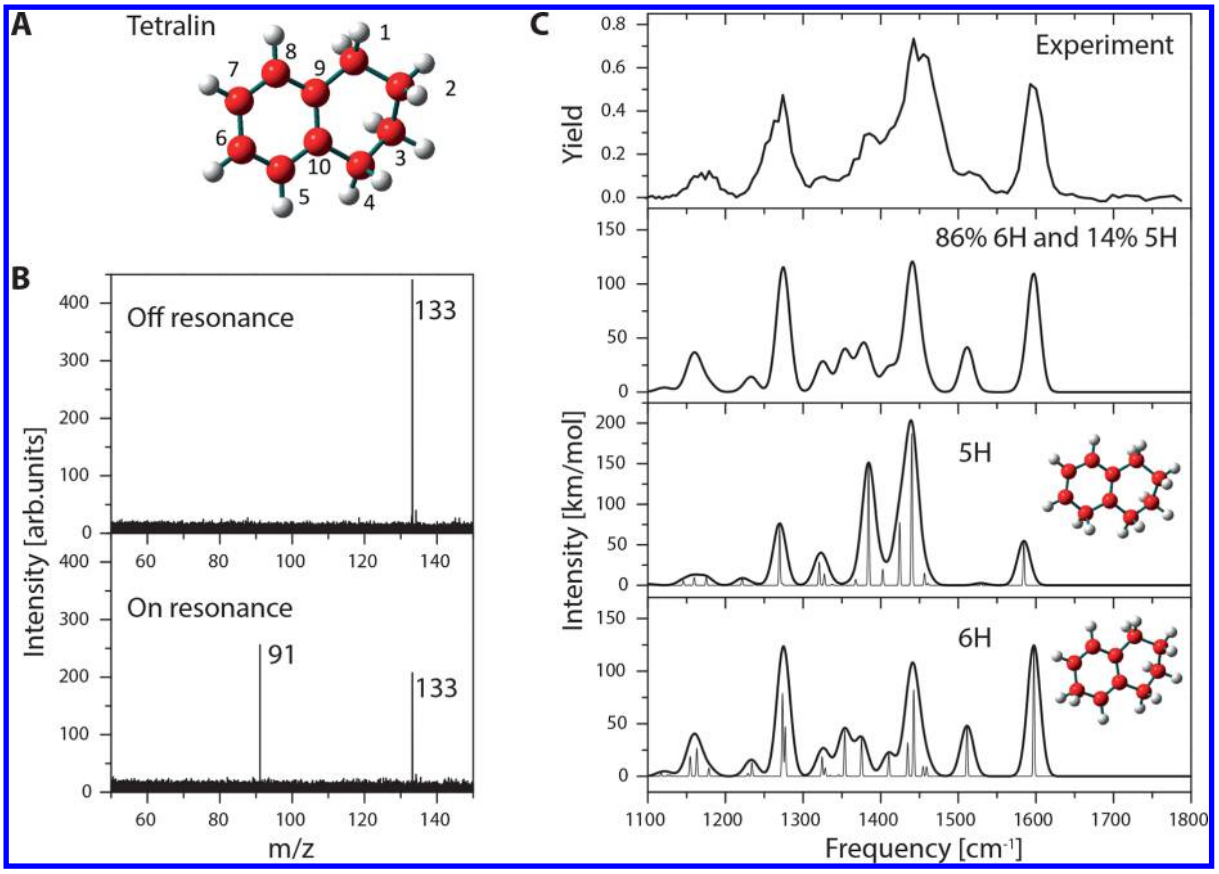

Figure 1. (a) Schematic diagram of tetralin (1,2,3,4-tetrahydronaphthalene) and the numbering scheme used. (b) Mass spectra recorded after irradiation with IR laser light with a frequency of 1700 cm^{-1} (off resonance) and 1600 cm^{-1} (on resonance). (c) Experimental IRMPD spectrum of protonated tetralin (top panel) and computed infrared absorption spectrum ((B3LYP/6-311++G(d,p) level) of tetralin protonated in the 6 position, $[THN + H(6)]^+$ (fourth panel) and protonated in the 5 position, $[THN + H(5)]^+$ (third panel). The second panel shows the spectrum obtained from a sum of $[THN + H(6)]^+$ and $[THN + H(5)]^+$ assuming a thermal distribution.

output in the infrared (Free Electron Laser for Infrared eXperiments (FELIX)).[17] The experimental apparatus has been previously described.[18] The protonated sample was formed by electrospray ionization of a 60:40 methanol/water solution of ~2 mM neutral THN with an infusion rate of ~30 μL/min. Ions were accumulated for 4 s in an rf hexapole trap and transferred to the ICR cell of the FTICR-MS. Here the protonated tetralin ions were mass-isolated and subsequently irradiated for 3 s by 30 infrared laser pulses of FELIX. In the range of 5.6−9 μm (1100−1800 cm^{-1}), the laser pulse energy was 15−50 mJ per 5 μs long macropulse (each of which comprises a group of picoseconds long pulses separated by 1 ns) and the bandwidth was 0.4% of the center frequency. When the IR laser frequency is resonant with a vibrational band of the protonated tetralin ion, absorption of multiple photons occurs thereby increasing its internal energy, which leads to unimolecular dissociation.[19−21] An IR spectrum of $[THN + H]^+$ was obtained by plotting the IRMPD yield, defined by the ratio of the number of IR photoinduced fragment ions and the total number of ions, as a function of the IR laser frequency. The yield was linearly corrected for the frequency-dependent laser power.

Molecular geometries and vibrational harmonic mode frequencies for all reactants, transition states (TSs), intermediates, and products were calculated using density functional theory with the Gaussian 03 program package.[22] Becke's three-parameter hybrid functional, the nonlocal correction functional of Lee, Yang, and Parr (B3LYP), with a 6-311++G(d,p) basis set were used.[23,24] The vibrational frequencies in the mid-IR range were scaled by a factor of 0.97 to correct for anharmonicity effects and functional/basis set deficiencies.

Potential energy profiles were computed using a B3LYP/6-31G level of theory, with single-point energy calculations carried out at the B3LYP/6-311++G(d,p) level (with zero-point energies included) for all reactant, transition state (TS), intermediate, and product structures. TS structures were identified by the presence of only a single imaginary frequency whose motion mimicked the reaction coordinates. QST2 calculations were carried out to pinpoint the TSs and intrinsic reaction coordinate computations were done to connect the reactant and product of each reaction step.

3. RESULTS AND DISCUSSION

Figure 1A shows a schematic of the parent tetralin (THN) molecule and the numbering scheme used. Protonation may occur at one of two unique sites on the aromatic ring (positions 5 and 6). Proton affinities computed for these two sites are very similar (8.425 eV for position 5 and 8.473 eV for position 6).

The IRMPD of protonated THN (m/z 133) produces only one fragment ion at m/z 91, as is shown in Figure 1B for irradiation at an IR frequency of 1600 cm^{-1}. No evidence for m/z 132 or 131 product fragments was found (also not at other frequencies), indicating no H or H_2 ejection from the

DOI: 10.1021/acs.jpca.7b01858
J. Phys. Chem. A 2017, 121, 4606−4612

protonated parent occurs. The m/z 91 peak corresponds to $C_7H_7^+$, with an ejected neutral C_3H_6 fragment.

The IRMPD spectrum of protonated THN was generated by plotting the ratio of the m/z 91 fragment yield over the sum of the m/z 91 fragment and m/z 133 parent intensities as a function of FELIX photon energy. Figure 1C shows the experimental spectrum together with the computed IR spectra for the two possible protonated isomers. Four major peaks are observed at 1174, 1274, 1451, and 1596 cm^{-1}. The computed spectrum for the $[THN + H(6)]^+$ isomer shows the same pattern for these bands with approximately the correct intensity ratios. Most importantly, only the spectrum for $[THN + H(6)]^+$ predicts a band in the 1500−1550 cm^{-1} region, which matches an observed band in this region. In addition, the observed band at 1150 cm^{-1} is also in accord with the predicted medium-intensity band in this region for the $[THN + H(6)]^+$ isomer. While this evidence points to the $[THN + H(6)]^+$ isomer as the predominant protonated species, we cannot rule out the presence of the $[THN + H(5)]^+$ isomer in some (smaller) percentage (*vide infra*). In fact, a better match to the experimental spectrum is obtained if we assume a thermal distribution over the two isomers, as is shown in Figure 1C, i.e., 86% $[THN + H(6)]^+$ and 14% $[THN + H(5)]^+$.

Three additional possible isomeric structures of protonated tetralin were computed in which one or more H shifts occur starting from $[THN + H(6)]^+$. They are the 1,2,3,5,*x* H-naphthalene cations (where x = 6, 7, and 8). For x = 6, a 1,3 H shift occurs from C(4) to C(5) in $[THN + H(6)]^+$. If then a 1,2 H shift occurs from C(6) to C(7), the x = 7 isomer is formed, and if a subsequent 1,2 H shift occurs from C(7) to C(8) the x = 8 isomer is produced. The calculations show that all these isomers are less stable than the $[THN + H(6)]^+$ isomer (see Table 1). More importantly, none of these isomers

Table 1. Relative Energies of Protonated Tetralin Isomers (1,2,3,*x*,*y*-H Naphthalene Cations)

x	*y*	relative energy (eV)
4	6	0.000
4	5	0.048
5	6	0.144
5	8	0.637
5	7	1.42[a]

[a]The x = 5, y = 7 isomer optimizes to a structure reminiscent of a methylene indane.

displays a band in the 1500−1550 cm^{-1} region, as is observed. In addition, the initial 1,3 H shift requires an input of ∼3.3 eV to reach the transition state, whereas protonation at the 5 or 6 position releases ∼8.4 eV energy. It therefore appears unlikely that these protonated isomers are present in the initial mixture of protonated tetralins.

Since the decomposition of protonated THN observed here yields one ionic product (m/z 91) and a neutral species corresponding to C_3H_6, ejection of a portion of the saturated ring of THN is clearly indicated. In the next section, the possible pathways computed for this dissociation are described, and in the following section, the computed isomerization/rearrangement of the m/z 91 product is illustrated.

A. Dissociation of Protonated Tetralin. While the infrared spectral evidence points to the $[THN + H(6)]^+$ isomer as the predominant protonated species, calculations were performed on both it and the $[THN + H(5)]^+$ species in order to determine whether the energy barriers to dissociation from the latter would preclude its contribution to the observed products. The overall scheme and reaction enthalpies for dissociation of the two isomers are given in Figure 2. Bond

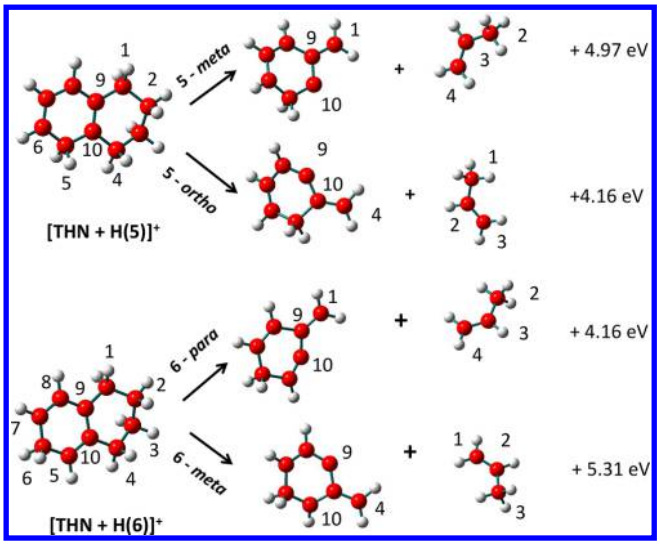

Figure 2. Schematic of the possible decomposition pathways for $[THN + H(5)]^+$ and $[THN + H(6)]^+$ and their computed reaction enthalpies. In the 5-*meta* and 6-*para* pathways, the C(1)−C(2) and C(4)−C(10) bonds are broken, while in the 5-*ortho* and 6-*meta* pathways, the C(1)−C(9) and C(3)−C(4) bonds are severed.

rupture may occur either at C(1)−C(2) and C(4)−C(10) or C(1)−C(9) and C(3)−C(4) in both isomers. The $C_7H_7^+$ products formed in the four possible breakdown pathways are different and are labeled 5-*meta*, 5-*ortho*, 6-*para*, and 6-*meta*, according to the relative positions of the methylene and hydro substituents around the ring. All computed reaction enthalpies (B3LYP/6-311++G(d,p)) are endothermic and in the +4.1−5.3 eV range. The barrier heights for these pathways were calculated as potential energy profiles. The relevant transition states, intermediate structures, and their relative energies, given in Figures 3 and 4, are discussed in turn below.

5-meta Pathway. Rupturing of the C(1)−C(2) bond in $[THN + H(5)]^+$ and separating these carbons to ∼2.7 Å results in transition state **TS1** in which H(3) straddles the C(2)−C(3) bond (see Figure 3a). A 1,2 H shift leads to methyl formation on C(2) and the subsequent closure of the C(2)−C(3)−C(4) arm to form the stable intermediate **A**, 3-methyl-5-hydro-indane.[25] With an additional input of 4.86 eV, the C(1)−C(3) and C(4)−C(10) bonds break and the $C_7H_7^+$ and C_3H_6 products formed. In the $C_7H_7^+$ product the methylene and extra hydro substituents are *meta* to each other, usually an unfavorable substituent configuration.

5-ortho Pathway. The more complex 5-*ortho* pathway is illustrated in Figure 3b. Here the C(3)−C(4) bond breaks and the carbons separate to ∼3.1 Å, after which **TS2** is formed with H(2) spanning the C(2)−C(3) bond. Stabilization results from methyl formation on C(3) followed by formation of the stable intermediate **B**. With a further input of 1.25 eV, **TS3** is formed, after which intermediate **C**, 1-methyl-5-hydro-indane, is produced. With a further input of 4.04 eV, the 5-*ortho* $C_7H_7^+$ product and C_3H_6 are produced. Overall this pathway requires +4.16 eV.

DOI: 10.1021/acs.jpca.7b01858
J. Phys. Chem. A 2017, 121, 4606−4612

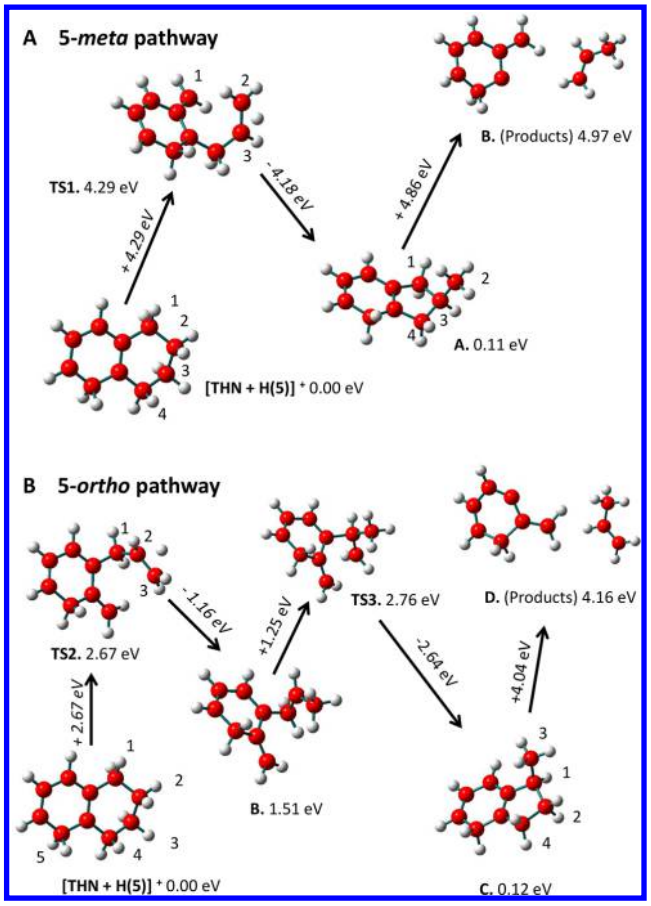

Figure 3. (a) Calculated potential energy profile (B3LYP/6-31G) with single-point geometries and energies, B3LYP/6-311++G(d,p) level (with zero-point energies included), for the decomposition of $[THN + H(5)]^+$ via the 5-*meta* pathway. (b) Calculated potential energy profile for the decomposition of $[THN + H(5)]^+$ via the 5-*ortho* pathway.

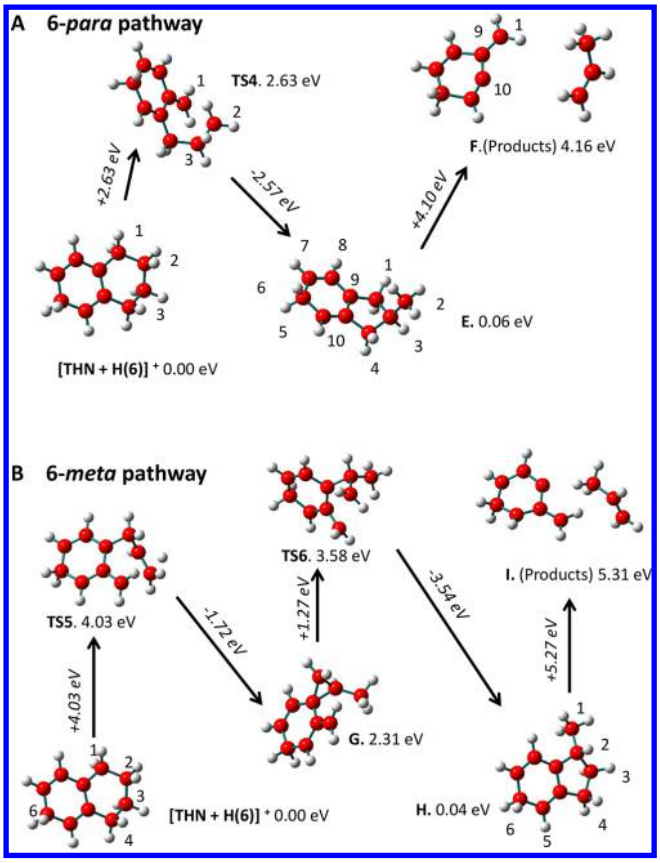

Figure 4. (a) Calculated potential energy profile (B3LYP/6-31G) with single-point geometries and energies, B3LYP/6-311++G(d,p) level (with zero-point energies included), for the decomposition of $[THN + H(6)]^+$ via the 6-*para* pathway. (b) Calculated potential energy profile for the decomposition of $[THN + H(6)]^+$ via the 6-*meta* pathway.

6-para Pathway. Along the 6-*para* path (Figure 4a), breaking the C(1)−C(2) bond in $[THN + H(6)]^+$ and separating these carbons to ∼3.5 Å leads to transition state **TS4**. Here the hydrogen from C(3) is midway between C(2) and C(3). A spontaneous 1,2 H shift to C(2) leads to methyl group formation. The pendant arm containing the methyl group then closes to form a five-membered ring, stabilizing to intermediate **E**, 3-methyl-6-hydro-indane.[25] With a further 4.10 eV input, the C(1)−C(3) and C(10)−C(4) bonds in **E** break, and the products $C_7H_7^+$ and C_3H_6 (propene, $CH_3C(H)=CH_2$) form. Overall this pathway requires +4.16 eV, a value equal to the thermodynamic value of +4.16 eV, and leaves the methylene and extra hydro substituents in a *para* configuration.

6-meta Pathway. Breaking the C(3)−C(4) bond and increasing its separation to ∼2.5 Å requires ∼4.0 eV, forming **TS5** (see Figure 4b). In this state the C(2) hydrogen undergoes a spontaneous 1,2 H shift to C(3). However, instead of forming an indane-like structure, a stable intermediate **G** with a spiro-attached three-membered ring is produced. The indane species **H** (2-methyl-6-hydro-indane)[25] is eventually formed from this intermediate after passing through **TS6**. Finally, the sought-after products are produced with an input of 5.27 eV. Overall, this pathway requires 5.31 eV.

Neither the calculated reaction enthalpies nor the potential energy barrier heights along the four reaction pathways outlined above permit one to conclusively exclude one or the other of these pathways. The initial barriers along two of the pathways (5-*ortho* and 6-*para*) are, however, ∼1.5 eV lower in energy than the other two, plus their total reaction enthalpies are 0.8−1.3 eV lower. Given the clear evidence from the IRMPD spectrum for the presence of the $[THN + H(6)]^+$ isomer, we conclude that the 6-*para* pathway is predominant and that the 5-*ortho* route may contribute a smaller, unknown percentage. For all pathways the energy required is identical to the thermodynamic value. The *ortho* or *para* $C_7H_7^+$ products are preferred over the *meta* products as is well-known from *ortho/para* directionality in electrophilic aromatic substitution reactions.

B. Rearrangement of the $C_7H_7^+$ (*m/z* 91) Product. The formation and isomerization of the $C_7H_7^+$ ion from a large number of alkylbenzene precursors has been the subject of extensive study.[26−46] In a 1994 review, Lifshitz pointed out that the first studies on the $C_7H_7^+$ ion, which utilized appearance potentials, hydrogen scrambling in deuterated precursors, and other thermochemical data, concluded that the tropylium ion was the final product.[26] Later work, however, presented evidence for the benzylium structure.[26−31] Very recent studies on the "thermometer" ion, benzylpyridinium ion, have inferred that the benzylium structure is formed first but later rearranges to form the tropylium structure.[32,33]

Here, the $C_7H_7^+$ (*m/z* 91) products from the four possible pathways are all isomers of the benzylium ion, dehydrogenated in one position and hydrogenated in another. As shown below, the energy requirements for rearrangement/isomerization to

DOI: 10.1021/acs.jpca.7b01858
J. Phys. Chem. A 2017, 121, 4606−4612

the benzylium ion are very modest and to the tropylium ion only slightly more so.

Figure 5 illustrates the route from the various benzylium-like products **D**, **I**, **F**, and **B** formed in the 5-*ortho*, 6-*meta*, 6-*para*, and 5-*meta* pathways, respectively, to the benzylium ion, **J**. This reaction scheme involves multiple 1,2 H shifts. From **D** to **J** requires four such shifts, while **B** to **J** requires just one. In the figure, product **D** is assigned a relative energy of 0.00 eV. Of the four benzylium-like products, **F** from the 6-*para* pathway is the lowest energy isomer, with **D** from the 5-*ortho* route only slightly higher. The highest barrier encountered along any of these reaction routes is ~1.5 eV.

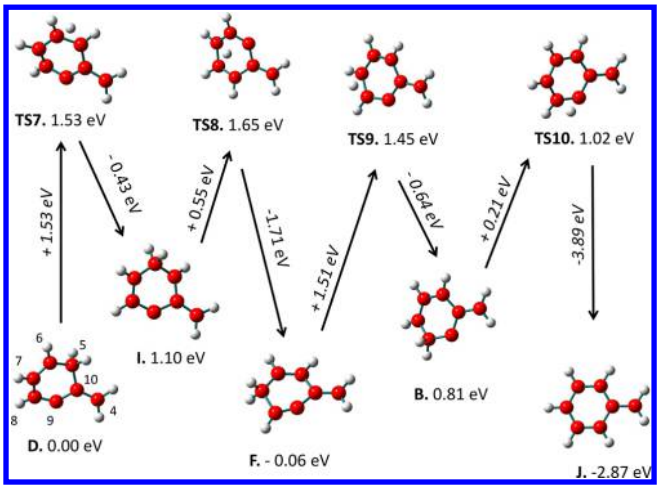

Figure 5. Computed potential energy profile for the rearrangement/isomerization of the $C_7H_7^+$ decomposition products **D**, **I**, **F**, and **B**, derived from the 5-*ortho*, 6-*meta*, 6-*para*, and 5-*meta* pathways, respectively, to the benzylium ion (**J**). Four 1,2 H shifts are required for the transformation of **D** to **J**, three for **I** to **J**, two for **F** to **J**, and one for **B** to **J** (all structures in the figure are singly charged cations).

Calculations were undertaken on an alternative, multistep pathway, which passes through a series of norcaradienyl-like structures. This path begins with the slight, out-of-plane twisting of the methylene group in the benzylium-like $C_7H_7^+$ product (such as **F**) to give the first transition state and then proceeds through a series of TSs and intermediates, all involving 1,2 H shifts. While the activation barriers found are all less than half as large as those in the direct route as in Figure 5, an intrinsic reaction coordinate (IRC) calculation showed that the first TS does not connect the twisted methylene transition state with the first norcaradienyl intermediate; thus, it can be concluded that this pathway is not viable. Such a conclusion has also been reached by Ignatyev and Sundius[41] and earlier by Smith and Hall.[34]

Turning to the tropylium ion, our approach toward its formation is similar to one originally proposed by Dewar and co-workers[44,45] and more recently expanded upon by Smith and Hall,[34] Ignatyev and Sundius,[41] and Kirkby and co-workers.[46] The latter authors calculated the formation of the tropylium ion from the toluene radical cation. Our calculation starts from **J**, the benzylium ion. Figure 6 shows that the methylene carbon C(1) bonds to the ring carbon C(8) creating the seven-membered ring **TS11**, which then stabilizes to compound **K**, the cycloheptatrienyl cation. A 1,2 H shift from C(1) to C(9) in **TS12** finally leads to the tropylium ion, **L**. The initial barrier from the benzylium ion to **TS11** is ~2.6 eV. The

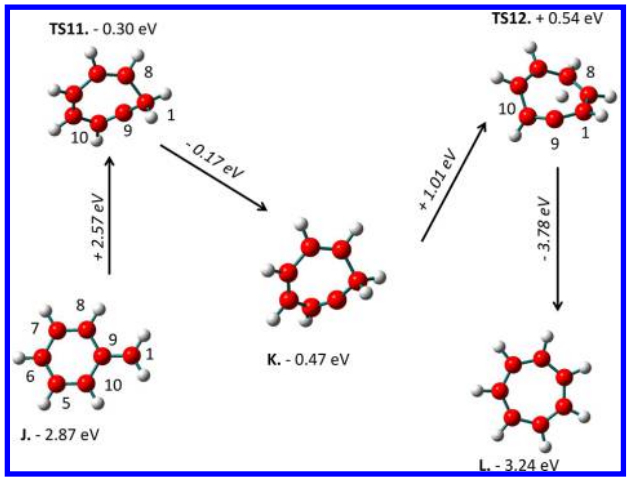

Figure 6. Computed potential energy profile for the conversion of the benzylium ion (**J**) to the tropylium ion (**L**).

tropylium ion is computed to be 0.37 eV more stable than the benzylium ion, a value equal to that found by Fridgen et al.[47]

If it had been possible to record an IRMPD spectrum of the m/z 91 product ion, this would directly identify whether the ion is in the benzylium or tropylium isomeric form. Although the entire population of protonated tetralin ions can be converted into m/z 91 using a 35 W continuous wave CO_2 laser, no further dissociation of the m/z 91 ions was observed, neither with FELIX nor with the CO_2 laser. This suggests that the m/z 91 ions are extremely stable, which prevents us from recording an IRMPD spectrum for this product ion.

4. CONCLUSIONS

The infrared multiple photon dissociation (IRMPD) spectrum of gaseous protonated tetalin (1,2,3,4-tetrahydronaphthalene) has been recorded using a Fourier-transform ion cyclotron resonance mass spectrometer (FTICR-MS) coupled to a free electron laser with tunable output in the infrared. Comparison of the observed spectrum of protonated tetralin with density functional calculations of the two possible protonation sites leads to the identification of its most probable position as 6, with position 5 less probable. Calculated potential energy profiles point to the 6-*para* pathway as the predominant route of the dissociation, with the 5-*ortho* route perhaps contributing a lesser percentage. In an effort to effect a closer fit to the experimental spectrum, a mixture of a number of different percentages of $[THN + H(6)]^+$ and $[THN + H(5)]^+$ were attempted. The best overall fit was achieved with a mixture of 86% $[THN + H(6)]^+$ and 14% $[THN + H(5)]^+$, which corresponds to a thermal distribution.

The 6-*para* pathway involves the spontaneous formation of a methyl group on the pendant saturated side arm followed by its subsequent closing to form the intermediate, 3-methyl-6-hydro-indane. The involvement of an indane intermediate in this decomposition reaction is consistent with the suggestion by McVickers and co-workers that, in the hydrogenation of naphthalene to tetralin, an equilibrium probably exists between tetralin and 1 (or 2)-methyl-indane and that the ring opening from the five-membered ring in indane is much faster than for the six-membered ring.[48] Finally, the computed energy profiles for the isomerization of the $C_7H_7^+$ ionic product lead to the conclusion that, given the relatively low barriers, the $C_7H_7^+$

DOI: 10.1021/acs.jpca.7b01858
J. Phys. Chem. A 2017, 121, 4606−4612

fragment product converts initially to the benzylium ion and, with sufficient activation, also to the tropylium ion.

Hydrogenated PAHs, while capable of producing molecular hydrogen, may also yield various breakdown products. The previous study[16] of 1,2-dihydronapthalene (DHN) with one partially hydrogenated ring showed that both H_2 and the breakdown product, benzylium/tropylium ion, were produced, while the present study of tetralin with a fully hydrogenated ring yields only the breakdown product. Earlier studies[14,15] on partially hydrogenated anthracene and phenanthrene (i.e., 9,10-dihydroanthracene (DHA) and 9,10-dihydrophenanthene (DHP)) produced evidence for the formation of molecular hydrogen. However, a very recent IRMPD investigation of the electron ionization-induced decomposition of the DHA and DHP ions has revealed a breakdown product, the fluorenyl ion, produced from each.[49] In the theoretical investigations of the DHN, DHA, and DHP parent ions, and the pathways leading to their respective breakdown products, a common intermediate was found. This intermediate, a five-membered ring with an attached methyl or methylene substituent, is formed from a partially (or fully) hydrogenated six-membered ring. It would be interesting to explore whether this type of intermediate is common in the destruction of other hydrogenated PAHs. Given the recently realized importance of hydrogenated PAHs and their role in the production of molecular hydrogen in the interstellar medium, further research seems warranted.

AUTHOR INFORMATION

Corresponding Author

*E-mail: mvala@chem.ufl.edu.

ORCID

Martin Vala: 0000-0003-3362-5122

Notes

The authors declare no competing financial interest.

ACKNOWLEDGMENTS

We greatly appreciate the skillful assistance of the FELIX facility staff. This work is part of the research program of FOM, which is financially supported by the Nederlandse Organisatie voor Wetenschappelijk Onderzoek (NWO).

REFERENCES

(1) Boschman, L.; Cazaux, S.; Spaans, M.; Hoekstra, R.; Schlathölter, T. H_2 Formation on PAHs in Photodissociation Regions: a High Temperature Pathway to Molecular Hydrogen. *Astron. Astrophys.* **2015**, *579*, A72−A83.

(2) Reitsma, G.; Boschman, L.; Deuzeman, M. J.; González-Magana, O.; Hoekstra, S.; Cazaux, S.; Hoekstra, R.; Schlathölter, T. Deexcitation Dynamics of Superhydrogenated Polycyclic Aromatic Hydrocarbon Cations after Soft x-Ray Excitation. *Phys. Rev. Lett.* **2014**, *113*, 053002.

(3) Mennella, V.; Hornekær, L.; Thrower, J.; Accolla, M. The Catalytic Role of Coronene for Molecular Hydrogen Formation. *Astrophys. J., Lett.* **2012**, *745*, L2−L7.

(4) Thrower, J. D.; Jørgensen, B.; Friis, E. E.; Baouche, S.; Mennella, V.; Luntz, A. C.; Andersen, M.; Hammer, B.; Hornekær, L. Experimental Evidence for the Formation of Superhydrogenated Polycyclic Aromatic Hydrocarbons through H Atom Addition and their Catalytic Role in H_2 Formation. *Astrophys. J.* **2012**, *752*, 3−8.

(5) Klærke, B.; Toker, Y.; Rahbek, D. B.; Hornekær, L.; Andersen, L. H. Formation And Stability Of Hydrogenated PAHs in the Gas Phase. *Astron. Astrophys.* **2013**, *549*, A84−A92.

(6) Omont, A. Physics and Chemistry of Interstellar Polycyclic Aromatic Molecules. *Astron. Astrophys.* **1986**, *164*, 159−178.

(7) Cassam-Chenai, N. P.; Pauzat, F.; Ellinger, Y. Is Stripping of Polycyclic Aromatic Hydrocarbons a Route to Molecular Hydrogen? *Am. Instit. of Physics Conf. Proc.* **1993**, *312*, 543−548.

(8) Pauzat, F.; Ellinger, Y. The 3.2−3.5 μm Region Revisited. II. A Theoretical Study of the Effects of Hydrogenation on Some Model PAHs. *Mon. Not. R. Astron. Soc.* **2001**, *324*, 355−366.

(9) Bauschlicher, C. W., Jr. The Reaction of Polycyclic Aromatic Hydrocarbon Cations with Hydrogen Atoms: The Astrophysical Implications. *Astrophys. J.* **1998**, *509*, L125−127.

(10) Hirama, M.; Tokosumi, T.; Ishida, T.; Aihara, J. Possible Molecular Hydrogen Formation Mediated by the Inner and Outer Carbon Atoms of Typical PAH cations. *Chem. Phys.* **2004**, *305*, 307−316.

(11) Ricca, A.; Bakes, E. L. O.; Bauschlicher, C. W., Jr. The Energetics for Hydrogen Addition to Naphthalene Cations. *Astrophys. J.* **2007**, *659*, 858−861.

(12) LePage, V.; Snow, T. P.; Bierbaum, V. M. Molecular Hydrogen Formation Catalyzed by Polycyclic Aromatic Hydrocarbons in the Interstellar Medium. *Astrophys. J.* **2009**, *704*, 274−280.

(13) Fu, Y.; Szczepanski, J.; Polfer, N. Photon-induced Formation of Molecular Hydrogen from a Neutral Polycyclic Aromatic Hydrocarbon: 9,10-Dihydroanthracene. *Astrophys. J.* **2012**, *744*, 61−68.

(14) Szczepanski, J.; Oomens, J.; Steill, J. D.; Vala, M. H_2 Ejection from Polycyclic Aromatic Hydrocarbons: Infrared Multiphoton Dissociation Study of Protonated Acenaphthene and 9,10-dihydrophenanthrene. *Astrophys. J.* **2011**, *727*, 12−25.

(15) Vala, M.; Szczepanski, J.; Oomens, J. Formation of Molecular Hydrogen from Protonated 9,10-Dihydroanthracene: Is the Ejected H_2 Rotationally and Vibrationally Excited? *Int. J. Mass Spectrom.* **2011**, *308*, 181−190.

(16) Vala, M.; Szczepanski, J.; Oomens, J.; Steill, J. D. H_2 Ejection from Polycyclic Aromatic Hydrocarbons: Infrared Multiphoton Dissociation Study of Protonated 1,2 Dihydronaphthalene. *J. Am. Chem. Soc.* **2009**, *131*, 5784−5791.

(17) Oepts, D.; van der Meer, A. F. G.; van Amersfoort, P. W. The Free-Electron-Laser User Facility FELIX. *Infrared Phys. Technol.* **1995**, *36*, 297−308.

(18) Valle, J. J.; Eyler, J.; Oomens, J.; Moore, D. T.; van der Meer, A. F. G.; von Helden, G.; Meijer, G.; Hendrickson, C. L.; Marshall, A. G.; Blakney, G. T. Free Electron Laser-Fourier Transform Ion Cyclotron Resonance Mass Spectrometry Facility for Obtaining Infrared Multiphoton Dissociation Spectra of Gaseous Ions. *Rev. Sci. Instrum.* **2005**, *76*, 023103.

(19) Polfer, N. C.; Oomens, J. Vibrational Spectroscopy of Bare and Solvated Ionic Complexes of Biological Relevance. *Mass Spectrom. Rev.* **2009**, *28*, 468−494.

(20) Polfer, N. C. Infrared Multiple Photon Dissociation Spectroscopy of Trapped Ions. *Chem. Soc. Rev.* **2011**, *40*, 2211−2221.

(21) Oomens, J.; Sartakov, B. G.; Meijer, G.; von Helden, G. Gas-Phase Infrared Multiple Photon Dissociation Spectroscopy of Mass-Selected Molecular Ions. *Int. J. Mass Spectrom.* **2006**, *254*, 1−9.

(22) Frisch, M. J.; Trucks, G. W.; Schlegel, H. B.; Scuseria, G. E.; Robb, M. A.; Cheeseman, J. R.; Zakrzewski, V. G.; Montgomery, J. A.; Stratmann, R. E., Jr.; Burant, J. C.; et al. *Gaussian 03*, revision B.05; Gaussian, Inc.; Pittsburgh, PA, 2003.

(23) Becke, A. D. Density-Functional Exchange-Energy Approximation with Correct Asymptotic Behavior. *Phys. Rev. A: At., Mol., Opt. Phys.* **1988**, *38*, 3098−3100.

(24) Lee, C.; Yang, W.; Parr, R. G. Development of the Cole-Salvetti Correlation-Energy Formula into a Functional of the Electron Density. *Phys. Rev. B: Condens. Matter Mater. Phys.* **1988**, *37*, 785−789.

(25) The numbering in the indane intermediates such as **A** (Figure 3a), **C** (Figure 3b), **E** (Figure 4a), and **H** (Figure 4b) are not the conventional ones used for indane derivatives, but reflect the original numbering in the parent ion. Conventional numbering, for example, for the indane derivative **A** is 2-methyl-5-hydro-indane, and for **C** is 1-methyl-5-hydro-indane.

DOI: 10.1021/acs.jpca.7b01858
J. Phys. Chem. A 2017, 121, 4606−4612

(26) Lifshitz, C. Tropylium Ion Formation from Toluene: Solution of an Old Problem in Organic Spectrometry. *Acc. Chem. Res.* **1994**, *27*, 138−144.
(27) Dunbar, R. C. Photodissociation of Toluene Parent Cation. *J. Am. Chem. Soc.* **1973**, *95*, 472−476.
(28) Hoffman, M. K.; Bursey, M. M. The Structure of the Molecular Ion of C_7H_8 Isomers: An ICR Study. *Tetrahedron Lett.* **1971**, *12*, 2539−2542.
(29) Winkler, J.; McLafferty, F. W. Metastable Ion Characteristics: XXX. Long-lived Benzyl and Tolyl Cations in the Gas Phase. *J. Am. Chem. Soc.* **1973**, *95*, 7533−7535.
(30) McLafferty, F. W.; Winkler, J. Metastable Ion Characteristics. XXXI. Gaseous Tropylium, Benzyl, Tolyl and Norbornadienyl Cations. *J. Am. Chem. Soc.* **1974**, *96*, 5182−5189.
(31) Shen, J.; Dunbar, R. C.; Olah, G. A. Gas Phase Benzyl Cations from Toluene Precursors. *J. Am. Chem. Soc.* **1974**, *96*, 6227−6229.
(32) Zins, E.-L.; Pepe, C.; Rondeau, D.; Rochut, S.; Galland, N.; Tabet, J.-C. Theoretical and Experimental Study of Tropylium Formation From Substituted Benzylpyridinium Species. *J. Mass Spectrom.* **2009**, *44*, 12−17.
(33) Morsa, D.; Gabelica, V.; Rosu, F.; Oomens, J.; De Pauw, E. Dissociation Pathways of Benzylpyridinium "Thermometer" Ions Depend on the Activation Regime: An IRMPD Spectroscopy Study. *J. Phys. Chem. Lett.* **2014**, *5*, 3787−3791.
(34) Smith, B. J.; Hall, N. E. G2(MP2,SVP) Study of the Relationship between the Benzyl and Tropyl Radicals, and the Cation Analogues. *Chem. Phys. Lett.* **1997**, *279*, 165−171.
(35) Fati, D.; Lorquet, A. J.; Locht, R.; Lorquet, J. C.; Leyh, B. Kinetic Energy Release for Tropylium and Benzylium Ion Formation from the Toluene Cation. *J. Phys. Chem. A* **2004**, *108*, 9777−9786.
(36) Choe, J. C. Dissociation of Toluene Cation: A New Potential Energy Surface. *J. Phys. Chem. A* **2006**, *110*, 7655−7662.
(37) Sekiguchi, O.; Mayer, V.; Letzel, M. C.; Kuck, D.; Uggerud, E. Energetics and Reaction Mechanisms for the Competitive Losses of H_2, CH_4 And C_2H_4 from Protonated Methylbenzenes-Implications to the Methanol-To-Hydrocarbons (MTH) Process. *Eur. Mass Spectrom.* **2009**, *15*, 167−181.
(38) Chiavarino, B.; Crestoni, M. E.; Fornarini, S.; Dopfer, O.; Lemaire, J.; Maitre, P. IR Spectroscopic Features of Gaseous $C_7O_7O^+$ Ions: Benzylium versus Tropylium Ion Structures. *J. Phys. Chem. A* **2006**, *110*, 9352−9360.
(39) Chiavarino, B.; Crestoni, M. E.; Dopfer, O.; Maitre, P.; Fornarini, S. Benzylium vs Tropylium Dichotomy: Vibrational Spectroscopy of Gaseous C_8H_9 Ions. *Angew. Chem., Int. Ed.* **2012**, *51*, 4947−4949.
(40) Zins, E.-L.; Pepe, C.; Schröder, D. Methylene-Transfer Reactions of Benzylium/Tropylium Ions with Neutral Toluene Studied by Means of Ion-Trap Mass Spectrometry. *Faraday Discuss.* **2010**, *145*, 157−169.
(41) Ignatyev, I. S.; Sundius, T. Competitive Hydride Shifts and Tolyl-Benzyl Rearrangements in Tolyl and Silatolyl Cations. *Chem. Phys. Lett.* **2000**, *326*, 101−108.
(42) Shin, C.-H.; Park, K.; Kim, S.-K.; Kim, B. Theoretical Approach for Equilibrium Structures and Relative Energies of the $C_7H_7^+$ Isomers and the Transition States between o-, m-, and p-Tolyl Cations. *Bull. Korean Chem. Soc.* **2002**, *23*, 337−345.
(43) Kim, S.-J.; Shin, C.-H.; Shin, S. K. *Ab initio* Quantum Mechanical Investigation of the Reaction Mechanisms of $C_7H_7^+$ from *o*-, *m*-, and *p*-Chlorotoluene Radical Cations. *Mol. Phys.* **2007**, *105*, 2541−2549.
(44) Cone, C.; Dewar, M. J. S.; Landman, D. Gaseous ions. I. MINDO/3 Study of the Rearrangement of Benzyl Cation to Tropylium. *J. Am. Chem. Soc.* **1977**, *99*, 372−376.
(45) Dewar, M. J. S.; Landman, D. Gaseous Ions. II. MINDO/3 Study of the Rearrangements of Toluene and Cycloheptatriene Molecular Ions and the Formation of Tropylium. *J. Am. Chem. Soc.* **1977**, *99*, 2446−2453.
(46) Bullins, K. W.; Huang, T. T. S.; Kirkby, S. Theoretical Investigation of the Formation of the Tropylium Ion from the Toluene Radical Cation. *Int. J. Quantum Chem.* **2009**, *109*, 1322−1327.
(47) Fridgen, T.; Troe, J.; Viggiano, A. A.; Midey, A. J.; Williams, S.; McMahon, T. B. Experimental and Theoretical Studies of the Benzylium$^+$/Tropylium$^+$ Ratios after Charge Transfer to Ethylbenzene. *J. Phys. Chem. A* **2004**, *108*, 5600−5609.
(48) McVickers, G. B.; Daage, M.; Touvelle, M. S.; Hudson, C. W.; Klein, D. P.; Baird, W. C., Jr.; Cook, B. R.; Chen, J. G.; Hantzer, S.; Vaughan, D. E. W.; Ellis, E. S.; Feeley, O. C. Selective Ring Opening of Naphthenic Molecules. *J. Catal.* **2002**, *210*, 137−148.
(49) Petrignani, A.; Vala, M.; Eyler, J. R.; Tielens, A. G. G. M.; Berden, G.; van der Meer, A. F. G.; Redlich, B.; Oomens, J. Breakdown Products of Gaseous Polycyclic Aromatic Hydrocarbons Investigated with Infrared Ion Spectroscopy. *Astrophys. J.* **2016**, *826*, 33.

DOI: 10.1021/acs.jpca.7b01858
J. Phys. Chem. A 2017, 121, 4606−4612